Fate and changes in moisture evaporated from the Tibetan Plateau (2000–2020)

Chi Zhang[1], Deliang Chen[2], Qiuhong Tang[3], Jinchuan Huang[4]

[1]Key Laboratory of Land Surface Pattern and Simulation, Institute of Geographic Sciences and Natural Resources Research, Chinese Academy of Sciences, Beijing, China

[2]Regional Climate Group, Department of Earth Sciences, University of Gothenburg, Gothenburg, Sweden

[3]Key Laboratory of Water Cycle and Related Land Surface Processes, Institute of Geographic Sciences and Natural Resources Research, Chinese Academy of Sciences, Beijing, China

[4]Key Laboratory of Regional Sustainable Development Modeling, Institute of Geographic Sciences and Natural Resources Research, Chinese Academy of Sciences, Beijing, China

Corresponding author: Jinchuan Huang (huangjc@igsnrr.ac.cn)

Key Points:

- The fate and changes of Tibetan Plateau evaporation were identified and quantified using an extended moisture tracking model
- 44.9–46.7% of Tibetan Plateau evaporation was recycled locally and about 2/3 of it was reprecipitated over terrestrial China
- Increased Tibetan Plateau evaporation was reprecipitated mainly around the northeast Plateau consistent with downwind precipitation changes

Abstract

Total evaporation from the vast terrain of the Tibetan Plateau (TP) may strongly influence downwind regions. However, the ultimate fate of this moisture remains unclear. This study tracked and quantified TP-originating moisture. The results show that the TP moisture participation in downwind regions' precipitation is the strongest around the eastern edge of the TP and then weakens gradually toward the east. Consequently, TP moisture in the composition of precipitation over the central-eastern TP is the largest of over 30%. 44.9–46.7% of TP annual evaporation is recycled over the TP, and about 2/3 of the TP evaporation is reprecipitated over terrestrial China. Moisture cycling of TP origin shows strong seasonal variation, with seasonal patterns largely determined by precipitation, evaporation and wind fields. High levels of evaporation and precipitation over the TP in summer maximize local recycling intensity and recycling ratios. Annual precipitation of TP origin increased mainly around the northeastern TP during 2000–2020. This region consumed more than half of the increased TP evaporation. Further analyses showed that

changes in reprecipitation of TP origin were consistent with precipitation trends in nearby downwind areas: when intensified TP evaporation meets intensified precipitation, more TP moisture is precipitated out. The model estimated an annual precipitation recycling ratio (PRR) of 26.9–30.8% in forward moisture tracking. However, due to the non-closure issue of the atmospheric moisture balance equation, the annual PRR in backward tracking can be ~6% lower.

1. Introduction

The Tibetan Plateau (TP) has been termed the "Asian water tower" and it plays an important role in regulating the Asian water cycle, which affects the lives of billions of people (Xu et al. 2014; Yao et al. 2022). In recent years, moisture cycling which concerns about the process of evaporation traveling through the atmosphere and returning to the surface as precipitation, has become a research hotspot in the TP hydrology. In revealing the local moisture recycling, i.e., the internal moisture cycling within the TP, Gao et al. (2020) obtained a distribution map of precipitation recycling ratios (PRRs; the fraction of precipitation contributed by local evaporation) across the TP using tracer analyses with a numerical weather forecasting model. They showed that the maximum PRR was located at the headwaters of three major rivers (Yangtze, Yellow and Mekong). Local recycling was much stronger in summer than in winter, and this difference was closely linked to convective precipitation (Gao et al. 2020). Using a bulk model with ERA5 reanalysis, Zhao and Zhou (2021) revealed that the interannual changes in PRR during 1979–2018 were mainly influenced by El Niño events through the anomalous Bengal Bay anticyclone. Using a dynamic recycling model and ERA5, He et al. (2021) demonstrated that the PRR increased at the rate of 0.07% yr^{-1} during 1979–2019. The local recycling was the main contributor (contributing 63.87%) to water vapor increases over the TP (He et al. 2021).

In addition to local moisture recycling, some recent studies have examined the external moisture sources to the TP. Using moisture backtracking in conjunction with satellite precipitation, Zhang (2020a) identified three major moisture sources for precipitation over the TP: the Southwest, corresponding to the South Asian summer monsoon (SASM); the West, corresponding to the westerlies from Europe; and local. Of these, the Southwest provided the greatest share of precipitation moisture, at around 31.9%. Moisture origins generally differ among climate subregions (Yao et al. 2013). In the northern TP, the westerlies dominated, providing 38.9% of precipitation moisture; in the southern TP, the SASM dominated, providing 51.4% of precipitation moisture (Zhang C et al. 2019). Similar results were obtained from analysis using the Community Atmosphere Model with an atmospheric water tagging technique (Pan et al. 2019). In the headwater region of the three major rivers in the TP, Zhang Y et al. (2019) tracked moisture trajectories using the HYSPLIT model and showed that moisture transfer paths from western and south-southeastern China were the most important for moderate to extreme precipitation of the region. In addition, recent increases in TP precipitation have been associated with its moisture sources

(Zhang et al. 2017; Li Y et al. 2019). It was found that most of the increased TP precipitation came from the Indian Ocean and the local TP (Zhang et al. 2017). Increased contributed moisture from the Indian Ocean was transported by the intensified SASM over the western Indian Ocean and increased moisture from local was generated through intensified local recycling (Zhang et al. 2017; Li Y et al. 2019).

Although the origins of the TP precipitated moisture have been relatively well studied, the fate of the TP evaporated moisture remains largely unknown. In an early study, Chen et al. (2012) tracked atmospheric moisture residing over the TP and developed a general overview of moisture destinations. However, the identified air parcel destinations were not directly linked to the moisture evaporated from the TP, that is, moisture in the tracked air parcels that left the TP might originate from outside. Due to the large scale of the TP, the total amount of evaporation can be substantial and may thus strongly influence precipitation downwind. Indeed, the distance traveled by TP moisture and the robustness of estimates for its internal recycling remain unclear. The spatial patterns and variations of the cycled TP moisture, i.e., precipitation of TP origin, especially during the rapid warming-and-wetting of the TP in recent decades, are of great scientific interest and deserve close examination.

To perform forward moisture tracking of evaporation over the TP, where ground observations are extremely rare, it is necessary to use model outputs and remote sensing products as basic data sources. It is very critical to assess uncertainties in these data and to choose the data used for tracking experiments. For variables with a large degree of uncertainty, multiple alternative datasets available can be used, and the sensitivity of a given simulation model to the input data can be measured using different combinations of the available datasets. Via deep analyses of the model algorithm, possible uncertainties due to the data or the model can be separated and quantified. In this study, we thus aim to 1) explore the destination of TP evaporation and to quantify the TP moisture involvement in downwind precipitation; 2) detect the recent change in the moisture receptors in relation to the recent increase in TP evaporation; and 3) assess uncertainties in the moisture tracking results related either to the input data or the model.

2. Materials and Methods

2.1. Data

Both atmospheric and surface-flux data are needed for the forward moisture tracking. For the atmospheric data, we used the latest reanalysis of ERA5, produced by the European Centre for Medium-Range Weather Forecasts (ECMWF; Hersbach et al. 2020). This dataset has been improved substantially in comparison to its predecessor (ERA-Interim) with respect to both modeling and assimilation technologies; the ERA5 dataset also incorporates more historical observations (Hersbach et al. 2020). The data include zonal and meridional winds, specific humidity at 23 pressure levels from 200 to 1000 hPa, surface pressure, total column water, and vertically integrated eastward and northward

atmospheric water fluxes. Atmospheric data are collected hourly at a resolution of 1°×1°.

The surface fluxes include evaporation and precipitation. Evaporation and precipitation in previous ECMWF reanalyses are type C variables purely determined by models (Dominguez et al. 2006; Berrisford et al. 2011). The updated ERA5 assimilates observational precipitation over the United States. However, in the current TP region, which lacks observational assimilation, it is better to choose more reliable products. It has been shown that evaporation over the TP is most accurately represented by the land surface model (LSM) NOAH in the Global Land Data Assimilation System-2.1 (GLDAS2.1) and the remote sensing (RS)-based product of the Global Land Evaporation Amsterdam Model (GLEAM) (Li X et al. 2019). They were thus applied in this study. GLDAS2.1 applies the upgraded Noah model (V3.6) which uses the modified IGBP MODIS 20-category vegetation classification. The adopted NOAH evaporation dataset is provided monthly at a scale of 0.25°×0.25° from 2000 to the present. GLEAM is a set of algorithms that separately estimate the different components of land evaporation, e.g., vegetation transpiration, bare-soil evaporation, and open-water evaporation (Martens et al. 2017). The adopted GLEAM v3.5a provides monthly total evaporation at 0.25°×0.25° from 1980 to 2020. Both NOAH and GLEAM TP evaporation series show significant upward trends during 2000–2020 in contrast to that of ERA5 (Fig. 1c).

The forcing precipitation of GLDAS2.1 NOAH is the 1°×1° Global Precipitation Climatology Project (GPCP) v1.3 Daily Analysis (Adler et al. 2020; Huffman et al. 2001), which was thus applied to match the NOAH evaporation. The daily GPCP data is based on multi-satellite observations and is scaled locally to add up to the GPCP Monthly (Adler et al. 2003). We also used a gauge-based precipitation dataset (CN05.1), produced by the National Climate Center of China Meteorological Administration (Wu and Gao 2013). This dataset integrates more than 2400 meteorological stations across China using the anomaly approach and is considered the best gridded precipitation data for China (Ma and Zhang 2022). The adopted CN05.1 is provided monthly from 1961 to 2021 at a scale of 0.25°×0.25°.

The ERA5 hourly evaporation and precipitation data were also retained to reflect diurnal variations in the temporal downscaling of the monthly products.

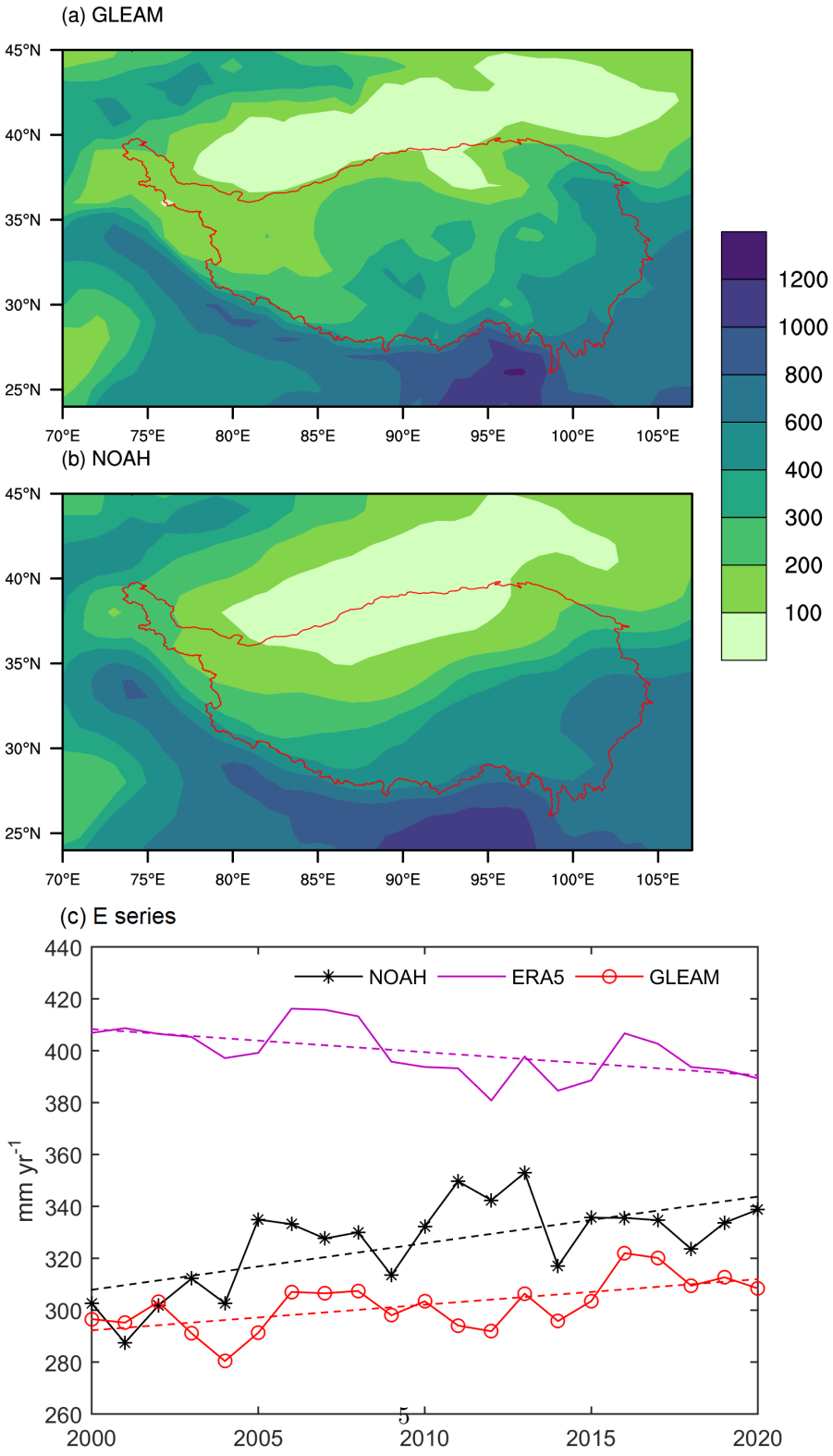
(a) GLEAM
45°N
40°N
35°N
30°N
25°N
70°E
75°E
80°E
85°E
90°E
95°E
100°E
105°E
1200
1000
800
600
400
300
200
100
(b) NOAH
(c) E series
NOAH
ERA5
GLEAM
mm yr-1
440
420
400
380
360
340
320
300
280
260
2000
2005
2010
2015
2020

Fig. 1. Annual evaporation over the Tibetan Plateau (TP; indicated by the red lines) from 2000 to 2020 with mean spatial distributions from (a) GLEAM and (b) NOAH (unit: mm yr^{-1}), as well as (c) interannual variations based on NOAH, GLEAM, and ERA5. The dashed lines correspond to the linear fit.

2.2. Model Extension and Experiment Design

WAM2Layers is a numerical moisture tracking model that can track moisture either forward or backward (van der Ent et al. 2013). It was driven by the model-level-based atmospheric reanalysis of ERA-Interim (Dee et al. 2013). To apply the pressure-level-based data of ERA5, some extensions were made. First, because the surface was not at the default pressure of 1000 hPa, linear interpolation and extrapolation were performed to calculate surficial variables at pressures smaller and larger than 1000 hPa, respectively. Wind speed at the surface was taken as zero. WAM2Layers divides the atmosphere into two layers at the 48th model level interface according to ERA-Interim. The corresponding pressure varies with surface pressure according to the following formula: $P_{\text{divide}} = 74.38 + 0.72879 \times P_{\text{surface}}$ (van der Ent et al. 2014). Based on this formula, the pressure at the divide interface is 812.83 hPa when the surface pressure is 1013.25 hPa. Since the chosen pressure levels were densely distributed in the lower atmosphere, we adopted the default pressure, which was the nearest to the division pressure, as the new division pressure. The horizontal moisture fluxes and column water vapor in the lower and upper compartments were computed accordingly.

All data were resampled into a 1°×1° grid first. The monthly GPCP precipitation values were obtained through the addition of the daily GPCP1.3. The hourly information in ERA5 evaporation and precipitation were used to downscale the monthly evaporation and precipitation to the hourly scale through proration (Zhang et al. 2017; Zhang 2020a). All hourly data, including both atmospheric and surface variables, were transformed into 15-minute intervals for model input.

In total, three groups of experiments were performed in this study. The atmospheric fields were derived solely from the ERA5 data. The experiments differed with respect to the combinations of evaporation and precipitation data used. The first evaporation-precipitation combination consisted of NOAH evaporation and GPCP precipitation (NOAH-GPCP); this combination reflected the results of the LSM model. The second combination consisted of GLEAM evaporation and GPCP precipitation (GLEAM-GPCP); both of these datasets are based on RS observations with ground validations or corrections. The third combination consisted of GLEAM evaporation and CN05.1 precipitation (GLEAM-CN). In this combination, the precipitation data over China in the global GPCP were replaced by the CN05.1 data, improving the reliability of the precipitation data in China. The tracking experiments were constrained to the overlapping period of data collection for all datasets (2000–2020).

3. Results

3.1. Annual TP Moisture Cycling

The cycled precipitation of TP origin is shown in Fig. 2. The center of cycled moisture is located near the eastern edge of the Plateau. As indicated by the 50% evaporationshed (i.e., the region that encloses the highest-valued cycled-precipitation grid squares that together account for 50% of the TP evaporation; van der Ent and Savenije 2013), moisture is concentrated over the TP and adjacent regions to the east. The moisture then expands eastward and slightly northward. This pattern demonstrated the important influence of the westerlies (Yasunari and Miwa 2006; Xu et al. 2019). The downwind northward-tilted distribution also reflected the influence of the southerly Asian monsoons (Wang and Chen 2012). The major 80% evaporationshed covered Korea and Japan to the Northwest Pacific in the east and covered Mongolia and China to Southeast Russia in the north. However, limited precipitation originating from the TP was found in the western TP. The 80% evaporationshed was about 5.7–6.3 times larger than the 50% evaporationshed, that is, ~6 times more area is needed to collect an additional 30% of the TP evaporated moisture.

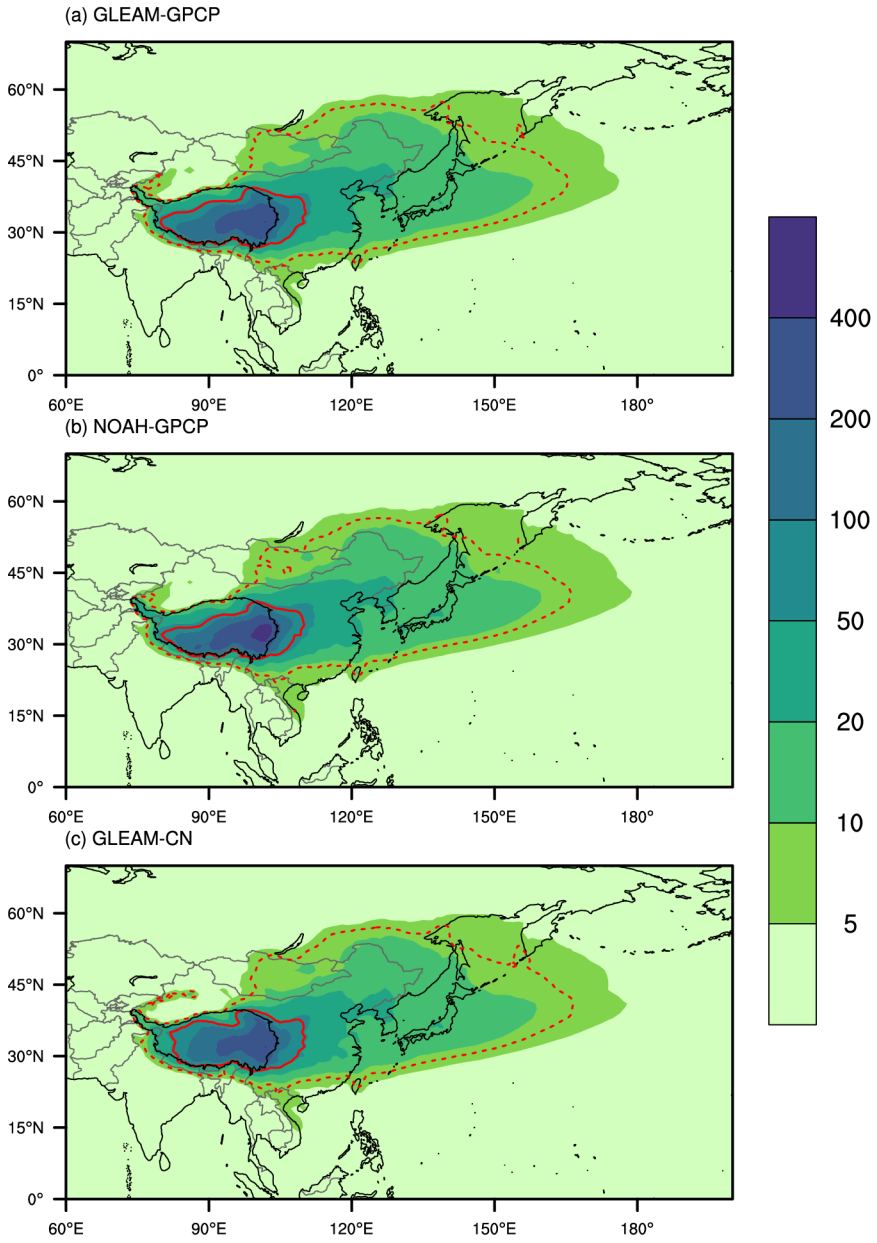

Fig. 2. Cycled precipitation originating from the TP from 2000 to 2020 using (a) GLEAM-GPCP, (b) NOAH-GPCP, and (c) GLEAM-CN (unit: mm yr^{-1}). The red solid and dashed lines mark the 50% and 80% evaporationsheds (van der Ent and Savenije 2013), respectively, containing the highest grid values for cycled precipitation.

To quantify recycling intensity over the TP, we calculated both the regional evaporation recycling ratio (ERR) and the PRR. Similar to the PRR, the ERR measures how much of the evaporated water returns to the source region as precipitation (van der Ent et al. 2010). The annual ERRs using GLEAM-GPP, NOAH-GPCP, and GLEAM-CN were calculated as 45.4±2.6%, 46.7±2.1%, and 44.9±2.7%, respectively. The estimates were quite consistent across dataset combinations, with little variation. In contrast, the annual PRRs calculated using GLEAM-GPP, NOAH-GPCP, and GLEAM-CN were fairly different (26.9±1.7%, 29.9±2.0%, and 30.8±1.6%, respectively). In addition to local moisture recycling, the cycled moisture in terrestrial China was also measured. Using GLEAM-CN, NOAH-GPCP, and GLEAM-GPCP, we estimated that the percentages of TP evaporation cycled within China were 65.1±1.9%, 66.8±1.7%, and 66.0±1.9%, respectively.

To quantify the importance of TP moisture to downwind regions, we calculated the contribution of TP moisture to precipitation across various regions (Fig. 3). There were few places where TP moisture accounted for more than half of the total precipitation. Precipitation containing high relative percentages of TP moisture (>30%) was concentrated over the central-eastern TP. Outside the TP, the TP moisture can't be viewed as a major precipitation source. The moisture gradient ellipses were oriented from the central-eastern TP toward Northeast China, demonstrating the relatively more important impact of TP moisture in the drier north than in the wetter south. Across all experiments, the 1% ratio line stretched eastward to Japan.

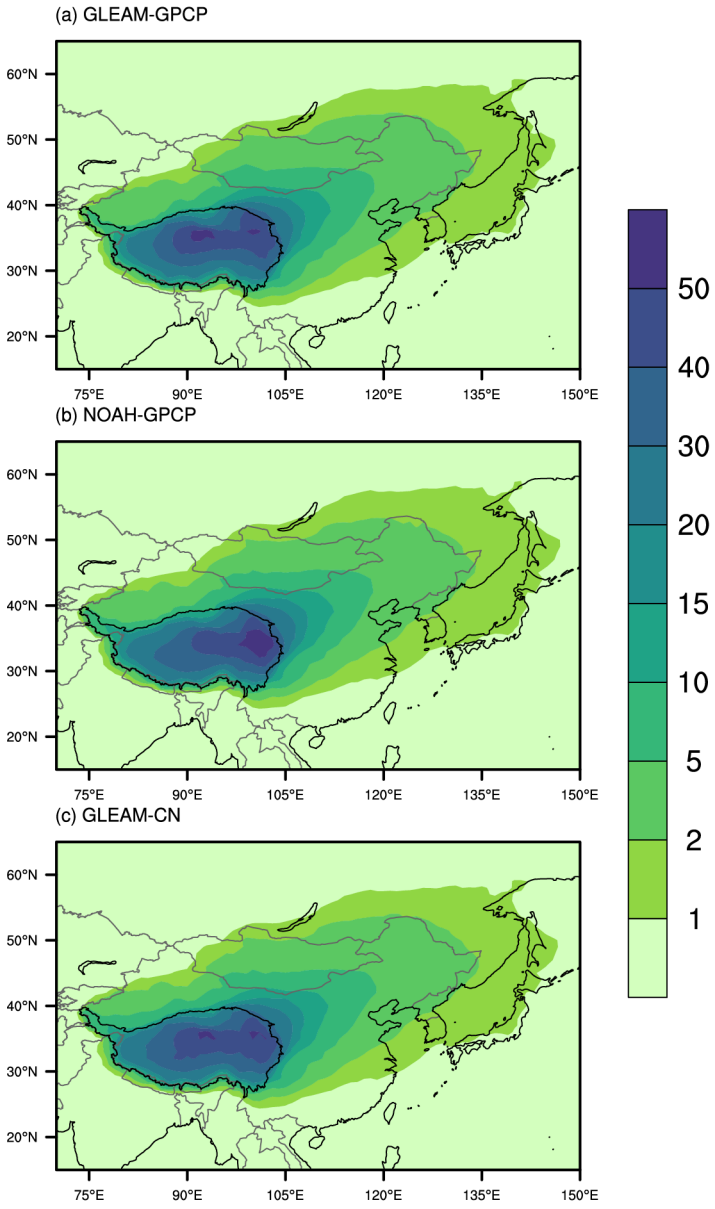

Fig. 3. Ratio of precipitation originating from the TP to total precipitation using (a) GLEAM-GPCP, (b) NOAH-GPCP, and (c) GLEAM-CN (unit: %).

3.2. Seasonal Variation in TP Moisture Cycling

Figure 4 shows the seasonal distributions of cycled TP moisture. Strong seasonal variations were identified in both magnitude and spatial distribution. For example, moisture cycling intensity was the weakest in winter due to low evap-

oration. In summer, evaporation on the TP was high, and the cycled moisture was maximized. According to the GLEAM-CN results, the cycled moisture in spring, summer, autumn, and winter accounted for 19.6±1.1%, 50.2±1.4%, 23.8±0.8%, and 5.3±0.4% of the annual evaporation, respectively.

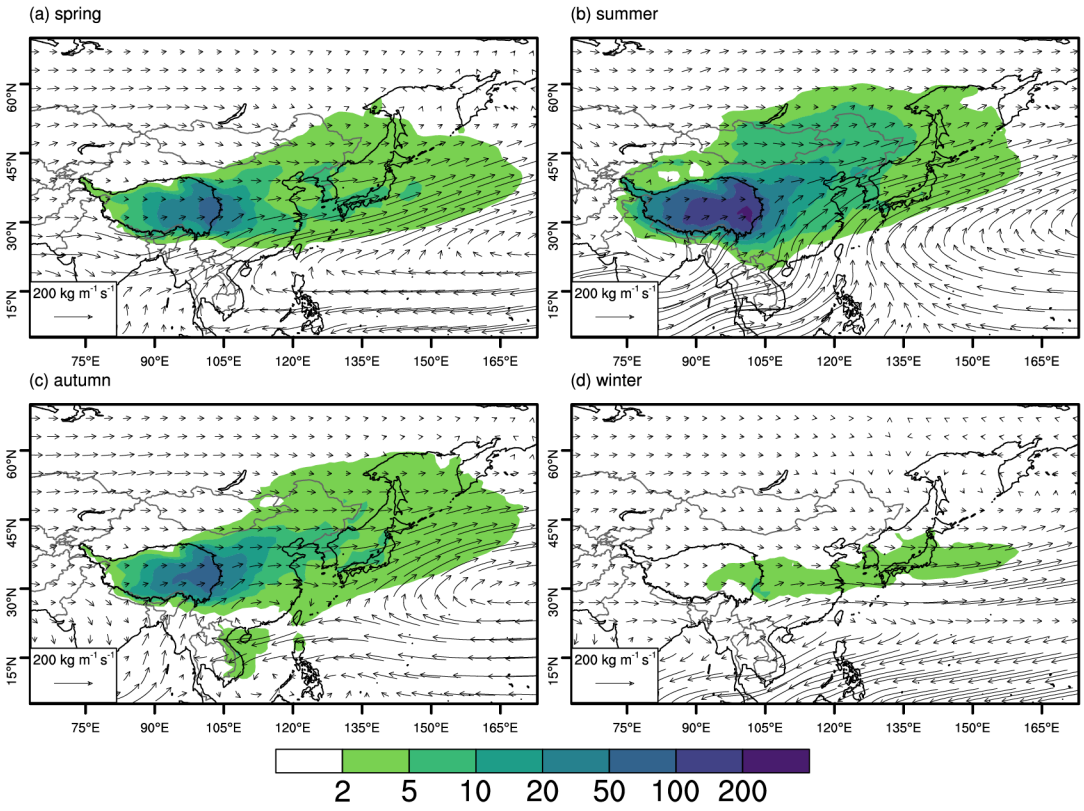

Fig. 4. Seasonal precipitation originating from the TP from 2000 to 2020, calculated using GLEAM-CN (unit: mm ssn^{-1}; ssn stands for season). The vectors represent seasonal, vertically integrated moisture transport.

In winter, the distribution of cycled moisture was almost zonal under the prevailing westerlies. In spring, due to the emergence of the Western Pacific Subtropical High (WPSH) (Wang et al. 2013), the zonal moisture flows were pushed a little bit northward at the lower downwind reaches, transporting TP moisture to Northeast China. In summer, due to the large-scale outbreak of the SASM (Ashfaq et al. 2009; Mitsui and Boers 2021) and the intensification of the WPSH (Zhu et al. 2018), the westerlies were pushed further northward, delivering more TP moisture over northern arid regions, such as Inner Mongolia and Mongolia itself. In autumn, when both the WPSH and the SASM retreat, the northward deflected TP-moisture was generally weaker. However, the subtropical high around the South China Sea (Wang et al. 2021) helps to steer the

TP moisture southward to the tropical through the formed anticyclone, leaving a well-marked water footprint at the coast of Vietnam (see also Fig. S2).

The seasonal ERRs and PRRs for the TP are shown in Fig. 5. Both indicators demonstrated that local moisture recycling is strong in summer and weak in winter (Gao et al. 2020; Yang et al. 2022). In autumn, local recycling was slightly stronger than in spring. In comparison with the PRRs, the ERRs were more convergent. In summer, more than half of the evaporation remained in the TP as reprecipitation, accounting for 30.5–34.1% of the total precipitation. The strong evaporation and precipitation in summer gave rise to the highest recycling ratios across all seasons (Yang et al. 2022).

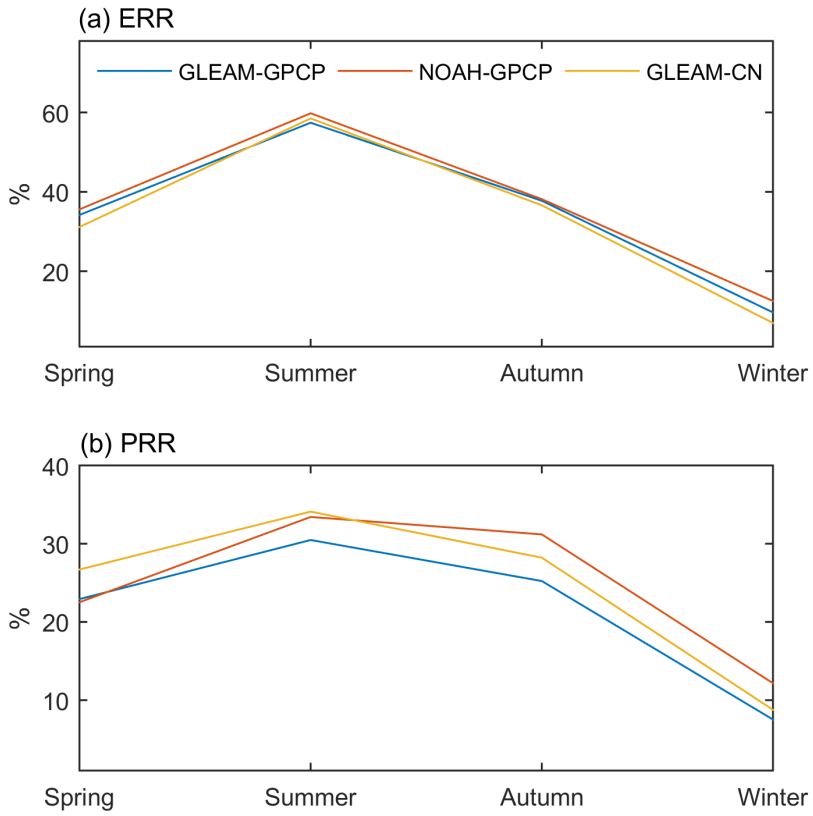

Fig. 5. Seasonal variations in (a) ERR and (b) PRR.

3.3. Changes in TP Moisture Cycling from 2000 to 2020

Evaporation over the TP increased significantly from 2000 to 2020 according to the NOAH and GLEAM data (Fig. 1), consistent with recently observed independent pieces of evidence, such as melting glaciers (Yao et al. 2019), ex-

panding lakes (Lei and Yang 2017), and greening vegetations (Zhong et al. 2019) associated with rapid warming over the TP (Lei and Yang 2017). However, the ultimate destination of this increased evaporation remains unclear. To address this knowledge gap, we calculated trends in cycled moisture over the past 21 years (Fig. 6). Since 2000, cycled moisture has increased dramatically and significantly around the northeastern TP. This finding was robust across all three experiments. Therefore, we focused more closely on the main region of cycled moisture increase (red marked region in Fig. 6) for further analyses.

Using GLEAM-GPCP and GLEAM-CN (Fig. 6a and 6c), we found that moisture in the main region increased at 7.7 and 6.6 mm yr^{-1} dec^{-1}, respectively, corresponding to 78.1% and 67.3% of the total increase in TP evaporation. Using NOAH-GPCP (i.e., Fig. 6b), we found that moisture in this region increased at 9.1 mm yr^{-1} dec^{-1}, which accounts for 50.9% of the total increase in TP evaporation. It was thus clear that the main increase region consumes the majority of the increased evaporation. It is also worth noting that a significant increase in cycled moisture was also identified at the lower reaches of the Yangtze River across all experiments. However, the magnitude of this increase was low.

To reveal the mechanisms underlying this increase in cycled TP moisture, the distribution of precipitation trends was analyzed (Fig. 7). The trend patterns over China recovered using GPCP1.3 and CN05.1 were similar, supporting the reliability of both datasets. Changes in cycled TP moisture seemed to be largely determined by changes in precipitation: in the main region of cycled moisture increase, we also observed a dramatic and significant increase in precipitation. This was likely because, when intensified evaporation meets intensified precipitation, more TP moisture is precipitated out. Although the increased precipitation belt extended to Northeast China (Fig. 7), the corresponding cycled moisture increase was much smaller than that in the main increase region (Fig. 6), because the increased TP moisture was quickly precipitated out, inhibiting the propagation of intensified TP evaporation. In the lower reaches of the Yangtze River, the precipitation rate increased much more sharply than in the main increase region, and the TP-originating precipitation similarly tended to increase significantly (Fig. 6). Although precipitation in southern China (specifically around the Guizhou and Guangxi provinces) also increased strongly (Fig. 7a), the corresponding cycled precipitation did not increase with the same intensity. Precipitation in this region originates primarily from the southwestern sources transported by the SASM (Zhang 2020b), where the TP moisture's influence is small.

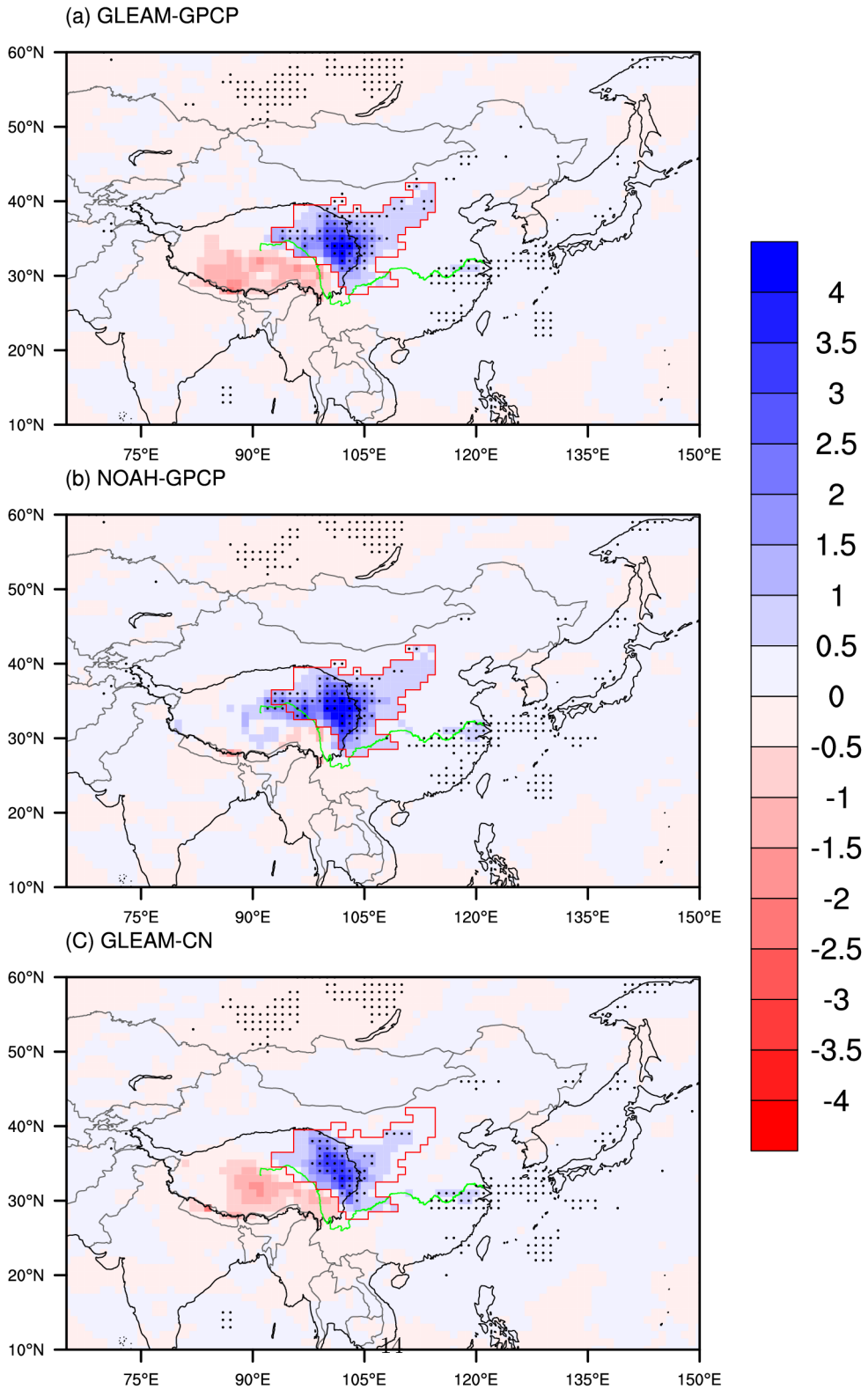
(a) GLEAM-GPCP
(b) NOAH-GPCP
(C) GLEAM-CN
60°N
50°N
40°N
30°N
20°N
10°N
75°E
90°E
105°E
120°E
135°E
150°E
4
3.5
3
2.5
2
1.5
1
0.5
0
-0.5
-1
-1.5
-2
-2.5
-3
-3.5
-4

Fig. 6. Trends in cycled precipitation of TP origin from 2000 to 2020, identified using (a) GLEAM-GPCP, (b) NOAH-GPCP, and (c) GLEAM-CN (unit: mm yr^{-1} dec^{-1}). The dots represent trends significant at the 0.05 level. The red rectangle indicates the main region of increase. The green line indicates the Yangtze River.

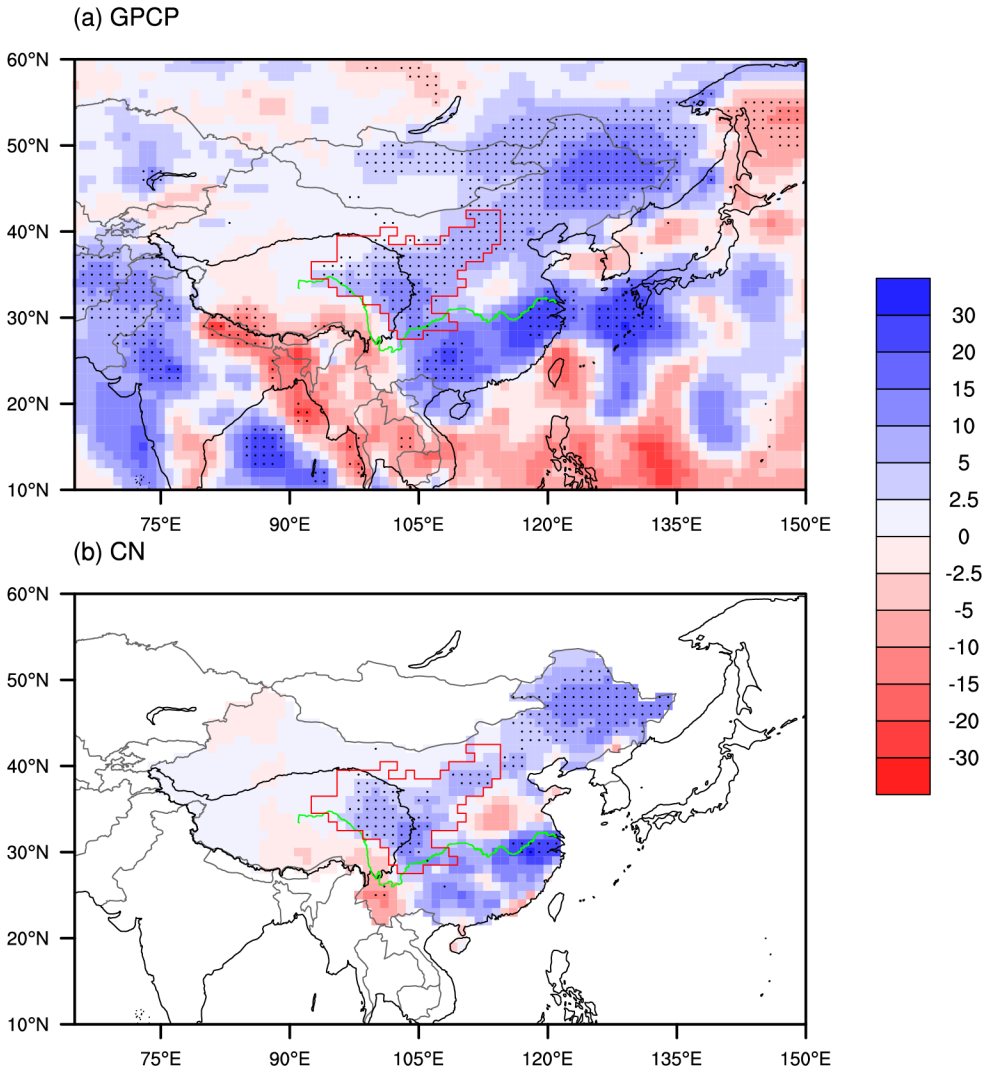

Fig. 7. Precipitation trends from 2000 to 2020 using (a) GPCP and (b) CN05.1 (unit: mm yr^{-1} yr^{-1}). The dots represent trends significant at the 0.05 level.

4. Discussion

4.1. Convergent ERRs but Divergent PRRs

ERR and PRR are important indicators that measure the interaction between land surface processes and atmospheric processes (Goessling and Reick 2011; van der Ent et al. 2010). In this study, the ERR values obtained from the three experiments were more convergent than the PRR values. For example, the ERRs calculated using GLEAM-GPCP and GLEAM-CN were similar: 45.4±2.6% and 44.9±2.7%, respectively. The two experiments used the same evaporation dataset (GLEAM), implying that the local recycled moisture values estimated were similar. In contrast, PRRs calculated using different precipitation datasets (i.e., GPCP1.3 and CN05.1) recovered dissimilar levels of TP precipitation (509.2±28.0 mm yr^{-1} and 439.7±22.8 mm yr^{-1}, respectively). Similar amounts of local recycled moisture also led to dissimilar PRRs. A PRR of 26.9±1.7% was recovered using GLEAM-GPCP, and a PRR of 30.8±1.6% was recovered using GLEAM-CN.

4.2. Model Uncertainty: Critical Thinking on the Tracking Algorithm

The use of different precipitation inputs resulted in a PRR variation of nearly 4%. We, therefore, attempted to look into the tracking process and determine how and why different input data influenced the results of the model. The WAM2Layers model is built upon the basic atmospheric moisture balance equation (van der Ent et al. 2010; 2014) as follows:

, (1)

where W represents the precipitable water contained in the air column; u and v represent the moisture mass-weighted zonal (x) and meridional (y) wind velocities, respectively; E represents evaporation; and P represents precipitation. Notably, all of these variables originate from different sources. Even though these variables are observational to a large extent, biases are inevitable. To make Equation 1 tenable in practice, a residual term is added to balance the equation (Eq. 2) as follows:

, (2)

where is the residual term. To calculate moisture of a specific origin, the expression is modified (Eq. 3) as follows:

, (3)

where Ω represents moisture with a given origin.

Here, as in other forward moisture tracking studies, TP-evaporated moisture is tagged in the air and flows with the winds. Only precipitation depletes tagged TP moisture from the air. When TP moisture is precipitated out, it is precipitated proportionally according to the mixed ratio W_Ω / W (Zhang et al. 2017; van der Ent et al. 2014). The remaining tagged moisture remains in the air until the next round of precipitation. Because the tagged water is precipitated proportionally throughout the process, if TP evaporation doubles while other fields and processes remain the same, the amount of cycled moisture should also double. Under this scenario, the ERR will remain unchanged, as the doubling

of local recycled moisture is counteracted by the doubled evaporation, but the PRR will double. Similarly, unilaterally increasing only the magnitude of precipitation will not affect PRR values but will change ERR values proportionally. Only when local evaporation and precipitation both increase in this situation, can the PRR and ERR values increase simultaneously.

During the tracking process in the model, the precipitable water at any time step cannot be balanced due to the existence of residual, which means that the precipitable water changes at the end of each time step. The tagged water, however, remains unchanged in the algorithm. This treatment ensures the conservation of tagged water during moisture cycling. However, as a result, local recycled moisture may differ between forward and backward tracking. To clarify, consider the entire TP as a single grid cell and simplify the two vertical layers into one. During a single time step, when the TP precipitable water changes from W_1 to W_2 in forward tracking, assume the existence of the positive residual $_1$, such that $W_1+e_1-p_1-\mathrm{div}(Q_1)+\ _1 = W_2$ (deduced from Eq. 2). At the time point of W_2, the model indicates that the ratio of the tagged water is e_1/W_2. However, we can also derive W_2' solely based on numerical computation of Equation 1, where $W_2' = W_1+e_1-p_1-\mathrm{div}(Q_1)$. Then, $W_2' = W_2-\ _1$. The mixed ratio of tagged water would be $e_1/(W_2-\ _1)$. During the following time step, with precipitation p_2, the tagged water produces cycled precipitation of $e_1/W_2\times p_2$ in the model and $e_1/(W_2-\ _1)\times p_2$ in the normal numerical computation. There is a tendency for the model algorithm to recover less cycled moisture than the normal numerical computation. However, in the backward tracking from W_2 to W_1, the mixed ratio of the tagged water at the time point of W_1 is p_1/W_1 in the model and $p_1/(W_1+\ _1)$ in the numerical computation. In the prior time step, with evaporation e_0, the cycled moisture is $p_1/W_1\times e_0$ and $p_1/(W_1+\ _1)\times e_0$ in the model and numerical computation, respectively. Thus, the model tracking tends to recover more cycled moisture than the normal numerical computation. The treatment of the residual term in WAM2Layers means that local recycled moisture content deviates reciprocally between forward and backward tracking, even using the same data set.

4.3. Data Uncertainty

Precipitation uncertainty has decreased in recent years due to the multiplication of surface gauges across the TP and the wide coverage of satellite observations. In contrast, the in-situ observations of evaporation are scarce (Li X et al. 2019). It is generally necessary to rely on RS-based or LSM-output evaporation products (Xin et al. 2022). The correlation coefficients between precipitation in GPCP1.3 and CN05.1 (Fig. 8b) indicate that variations in precipitation are reliable at the grid scale, although the data for the TP were less similar between datasets in comparison to the rest of China. In contrast, correlation between GLEAM3.5 and NOAH (Fig. 8a) evaporations is relatively poor, with many negatively correlated grid squares across the TP. It has been argued that GLEAM, which relies on calculations of potential evaporation, might perform poorly in arid and semiarid regions (Li X et al. 2019). However, as shown in Fig. 8a,

GLEAM performs well not only in humid India but also in arid North China. If RS-based algorithms are applicable in various regions, they might also be applicable in the TP, as such algorithms are more generalized than LSMs. The methods used to compute evaporation in LSMs differ from those of GLEAM, as LSMs rely on multiple land surface processes. However, over such a complex terrain with substantial glacial coverage, LSM models are limited because our understanding of the relevant physical processes and the model parameterizations is not mature (Ma et al. 2022). Thus, the estimated moisture cycling results based on GLEAM evaporation values may be considered reliable.

Recently, Ma and Zhang (2022) estimated the monthly evaporation of the TP from 1982 to 2016 using a water-carbon-coupled RS-based model, and all month-scale variables were input to the Penman-Monteith equation. However, because evaporation intensity has a strong diurnal cycle, it is questionable whether monthly variables/parameters accurately represent evaporation. Ma and Zhang (2022) estimated a TP evaporation of around 350 mm yr^{-1}, which was somewhat greater than the values calculated using NOAH (~325 mm yr^{-1}) and GLEAM (~300 mm yr^{-1}). If Ma and Zhang's quantification is more reliable than the previous two, we can probably predict changes in cycled moisture based on current simulations. Previous analyses demonstrated that unilateral increases in the magnitude of evaporation increase cycled moisture by an equivalent proportion. Consequently, the ERR remains unchanged, but the PRR increases. In addition, the relative contribution of TP moisture to downwind precipitation becomes proportionally larger as TP evaporation increases.

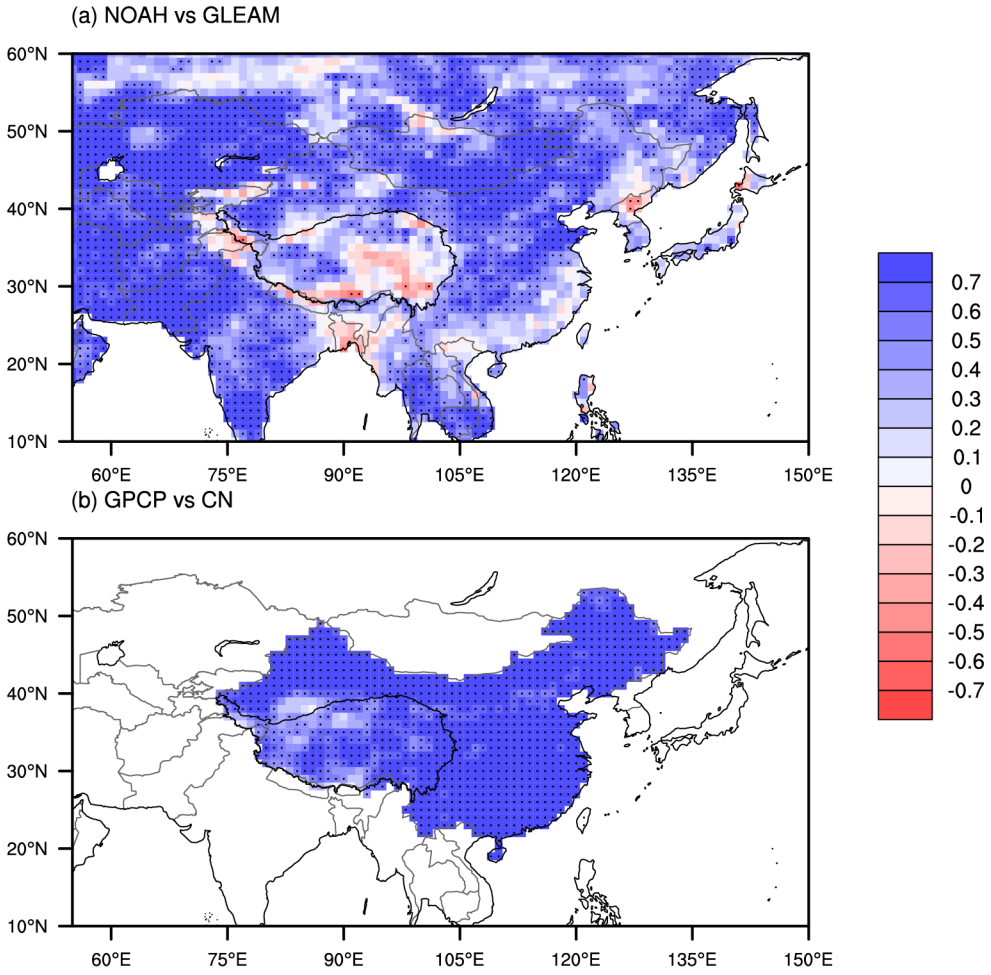

Fig. 8. Correlations (a) between NOAH- and GLEAM-derived evaporation values and (b) between GPCP- and CN05.1-derived precipitation values. All series were linearly detrended before analysis. Dots indicate significant correlations (P-value < 0.05).

In this study, we estimated an annual PRR of 26.9–30.8% and a summer PPR of 30.5–34.1%. Recently, Zhao and Zhou (2021) estimated a summer PRR of around 23% in the TP based on the bulk model and ERA5 reanalysis, while He et al. (2021) estimated a summer PRR of 24.2% using the dynamic recycling model. In contrast, Gao et al. (2020) calculated a PRR of up to ~40% in summer months based on a regional climate model. PRR values may vary depending on several factors, including size of the region considered, climate regime, season and time, the applied data, and the calculation methods used (Yang et al. 2022). In the moisture tracking experiments, we tracked the evaporated moisture consecutively for a whole year. The recycled precipitation in

summer TP could originate partly from antecedent evaporation in spring. However, this part of moisture was not accounted for in Zhao and Zhou (2021) or He et al. (2021). Our estimates of summer PRRs are thus larger. In addition, due to the existence of the residual term, different tracking modes in WAM2Layers can result in divergent values for local recycled moisture, which may lead to incongruence in the PRR or the ERR. In a backward-tracking precipitation study, Zhang (2020a) estimated an annual PRR of 23.6±2.3% between 1998 and 2018. To further quantify the uncertainty caused by the residual in different tracking modes, we performed an additional experiment using the backtracking mode with the NOAH-GPCP dataset and calculated an average PRR of 23.8±1.1%. In contrast, the PRR obtained using the same data set but with forward tracking was 29.9±2.0%. Thus, the uncertainty range in the PRR can be as large as ~6%.

Uncertainty exists not only in precipitation and evaporation datasets but also in the atmospheric fields of precipitable water and wind (Wang et al. 2017; Ding et al. 2021). As technology continues to advance, it is believed that observational biases will decrease concomitantly, eventually reducing the residual term to a minimum and leading to more convergent results.

5. Summaries and Conclusions

The fate of TP evaporation during 2000–2020 has been explored using the extended version of WAM2Layers. In order to constrain the uncertainty caused by input data especially the TP evaporation, some best-performed products such as GLEAM3.5 and NOAH (GLDAS2.1) were applied and formed into various data combinations to force the model. According to the results, 44.9–46.7% of annual TP evaporation is recycled over the TP, and about 2/3 of the TP evaporation is reprecipitated over terrestrial China. Within China, TP-evaporated moisture is reprecipitated the strongest around the eastern edge of the TP. Outside China, TP moisture is mostly precipitated over South Korea, North Korea, and Japan.

TP moisture cycling shows strong seasonal variation, which comes to full flourish in summer but becomes wilted in winter. The seasonal patterns are largely determined by precipitation, evaporation and wind fields. High levels of evaporation and precipitation over the TP in summer maximize the local recycling intensity and recycling ratios. In statistics, more than half of the summer evaporation recycles in the TP, accounting for 30.5–34.1% of the total precipitation.

TP evaporation increased significantly during the study period. The increased moisture was precipitated mainly around the northeastern TP. Across all experiments, this region consumed more than half of the increased TP evaporation. It was found that changes in reprecipitation of TP evaporation were largely determined by precipitation trends in nearby downwind areas. When intensified TP evaporation meets intensified precipitation, more TP moisture is precipitated out.

Deep analyses into the cycling process reveal that unilaterally changing the evaporation magnitude only changes the corresponding cycled moisture content in

proportion, thus enlightening future applications if more advanced evaporations emerge. However, the non-closure issue in the atmospheric moisture balance equation can be really serious in moisture tracking as it introduces the uncertainty rooted in the model. In the forward tracking using NOAH-GPCP, the annual PRR was estimated to be 29.9±2.0%. Using the same data, the PRR was 23.8±1.1% in the backward tracking. Future researches should be cautious in interpreting these results and take this model uncertainty into account when the residual term in the atmospheric moisture equation is non-negligible.

Acknowledgements.

Special thanks are given to Ruud van der Ent from Delft University of Technology, the author of WAM2Layers, for providing the original WAM2Layers code. We also thank Aqeel Ahmad from the Institute of Geographic Sciences and Natural Resources Research, Chinese Academy of Sciences and Binod Baniya from Tribhuvan University for language editing. This work was supported by the National Natural Science Foundation of China (grant number 41701033). The authors declare that they have no conflict of interest.

Data Availability Statement.

All data applied in this study are public which can be freely downloaded from the official websites. The modelled and resultant data that support this study are available upon request from C. Zhang (zhangchi@igsnrr.ac.cn).

References

Adler, R. F., Wang, J., Sapiano, M., Huffman, G., Bolvin, D., Nelkin, E., & NOAA CDR Program (2020). Global Precipitation Climatology Project (GPCP) Climate Data Record (CDR), Version 1.3 (Daily). Research Data Archive at the National Center for Atmospheric Research, Computational and Information Systems Laboratory, accessed 14 January 2022. https://doi.org/10.5065/ZGJD-9B02

Adler, R. F., Huffman, G. J., Chang, A., Ferraro, R., Xie, P.-P., Janowiak, J., et al. (2003). The Version-2 Global Precipitation Climatology Project (GPCP) Monthly Precipitation Analysis (1979–Present). *Journal of Hydrometeorology*, *4*(6), 1147–1167. https://doi.org/10.1175/1525-7541(2003)004<1147:TVGPCP>2.0.CO;2

Ashfaq, M., Shi, Y., Tung, W., Trapp, R. J., Gao, X., Pal, J. S., & Diffenbaugh, N. S. (2009). Suppression of south Asian summer monsoon precipitation in the 21st century. *Geophysical Research Letters*, *36*(1). https://doi.org/10.1029/2008GL036500

Berrisford, P., Kållberg, P., Kobayashi, S., Dee, D., Uppala, S., Simmons, A. J., et al. (2011). Atmospheric conservation properties in ERA-Interim. *Quarterly Journal of the Royal Meteorological Society*, *137*(659), 1381–1399. https://doi.org/10.1002/qj.864

Chen, B., Xu, X.-D., Yang, S., & Zhang, W. (2012). On the origin and destination of atmospheric moisture and air mass over the Tibetan Plateau. *Theoretical and Applied Climatology*, *110*(3), 423–435.

Dee, D. P., Uppala, S. M., Simmons, A. J., Berrisford, P., Poli, P., Kobayashi, S., et al. (2011). The ERA-Interim reanalysis: configuration and performance of the data assimilation system. *Quarterly Journal of the Royal Meteorological Society*, *137*(656), 553–597. https://doi.org/10.1002/qj.828

Ding, J., Cuo, L., Zhang, Y., & Zhang, C. (2021). Varied spatiotemporal changes in wind speed over the Tibetan Plateau and its surroundings in the past decades. *International Journal of Climatology*, *41*(13), 5956–5976.

Dominguez, F., Kumar, P., Liang, X.-Z., & Ting, M. (2006). Impact of atmospheric moisture storage on precipitation recycling. *Journal of Climate*, *19*(8), 1513–1530.

van der Ent, R. J., Tuinenburg, O. A., Knoche, H.-R., Kunstmann, H., & Savenije, H. H. G. (2013). Should we use a simple or complex model for moisture recycling and atmospheric moisture tracking? *Hydrology and Earth System Sciences*, *17*(12), 4869–4884.

van der Ent, R. J., Wang-Erlandsson, L., Keys, P. W., & Savenije, H. H. G. (2014). Contrasting roles of interception and transpiration in the hydrological cycle–Part 2: Moisture recycling. *Earth System Dynamics*, *5*(2), 471–489.

van der Ent, Rudi J., & Savenije, H. H. (2013). Oceanic sources of continental precipitation and the correlation with sea surface temperature. *Water Resources Research*, *49*(7), 3993–4004.

van der Ent, Rudi J., Savenije, H. H., Schaefli, B., & Steele-Dunne, S. C. (2010). Origin and fate of atmospheric moisture over continents. *Water Resources Research*, *46*(9), W09525.

Gao, Y., Chen, F., Miguez-Macho, G., & Li, X. (2020). Understanding precipitation recycling over the Tibetan Plateau using tracer analysis with WRF. *Climate Dynamics*, *55*(9), 2921–2937. https://doi.org/10.1007/s00382-020-05426-9

Goessling, H. F., & Reick, C. H. (2011). What do moisture recycling estimates tell us? Exploring the extreme case of non-evaporating continents. *Hydrology and Earth System Sciences*, *15*(10), 3217–3235.

He, Y., Tian, W., Huang, J., Wang, G., Ren, Y., Yan, H., et al. (2021). The mechanism of increasing summer water vapor over the Tibetan Plateau. *Journal of Geophysical Research: Atmospheres*, *126*(10), e2020JD034166.

Hersbach, H., Bell, B., Berrisford, P., Hirahara, S., Horányi, A., Muñoz-Sabater, J., et al. (2020). The ERA5 global reanalysis. *Quarterly Journal of the Royal Meteorological Society*, *146*(730), 1999–2049.

Huffman, G. J., Adler, R. F., Morrissey, M. M., Bolvin, D. T., Curtis, S., Joyce, R., et al. (2001). Global precipitation at one-degree daily resolution from

multisatellite observations. *Journal of Hydrometeorology*, *2*(1), 36–50.

Immerzeel, W. W., Van Beek, L. P., & Bierkens, M. F. (2010). Climate change will affect the Asian water towers. *Science*, *328*(5984), 1382–1385.

Lei, Y., & Yang, K. (2017). The cause of rapid lake expansion in the Tibetan Plateau: climate wetting or warming? *Wiley Interdisciplinary Reviews: Water*, *4*(6), e1236.

Li, X., Long, D., Han, Z., Scanlon, B. R., Sun, Z., Han, P., & Hou, A. (2019). Evapotranspiration estimation for Tibetan Plateau headwaters using conjoint terrestrial and atmospheric water balances and multisource remote sensing. *Water Resources Research*, *55*(11), 8608–8630.

Li, Y., Su, F., Chen, D., & Tang, Q. (2019). Atmospheric water transport to the endorheic Tibetan Plateau and its effect on the hydrological status in the region. *Journal of Geophysical Research: Atmospheres*, *124*(23), 12864–12881.

Ma, N., & Zhang, Y. (2022). Increasing Tibetan Plateau terrestrial evapotranspiration primarily driven by precipitation. *Agricultural and Forest Meteorology*, *317*, 108887.

Ma, Y., Wang, B., Chen, X., Zhong, L., Hu, Z., Ma, W., et al. (2022). Strengthening the three-dimensional comprehensive observation system of multi-layer interaction on the Tibetan Plateau to cope with the warming and wetting trend. *Atmospheric and Oceanic Science Letters*, *15*(4), 100224.

Martens, B., Miralles, D. G., Lievens, H., Van Der Schalie, R., De Jeu, R. A., Fernández-Prieto, D., et al. (2017). GLEAM v3: Satellite-based land evaporation and root-zone soil moisture. *Geoscientific Model Development*, *10*(5), 1903–1925.

Mitsui, T., & Boers, N. (2021). Seasonal prediction of Indian summer monsoon onset with echo state networks. *Environmental Research Letters*, *16*(7), 074024.

Pan, C., Zhu, B., Gao, J., Kang, H., & Zhu, T. (2019). Quantitative identification of moisture sources over the Tibetan Plateau and the relationship between thermal forcing and moisture transport. *Climate Dynamics*, *52*(1), 181–196.

Wang, H., & Chen, H. (2012). Climate control for southeastern China moisture and precipitation: Indian or East Asian monsoon? *Journal of Geophysical Research: Atmospheres*, *117*(D12), D12109.

Wang, L., Qian, Y., Leung, L. R., Chen, X., Sarangi, C., Lu, J., et al. (2021). Multiple Metrics Informed Projections of Future Precipitation in China. *Geophysical Research Letters*, *48*(18), e2021GL093810. https://doi.org/10.1029/2021GL093810

Wang, L.-W., Zheng, F., & Zhu, J. (2013). Predicting Western Pacific Subtropical High Using a Combined Tropical Indian Ocean Sea Surface Temperature Forecast. *Atmospheric and Oceanic Science Letters*, *6*(6), 405–409. https://doi.org/10.3878/j.issn.1674-2834.13.0030

Wang, Y., Yang, K., Pan, Z., Qin, J., Chen, D., Lin, C., et al. (2017). Evaluation of precipitable water vapor from four satellite products and four reanalysis datasets against GPS measurements on the Southern Tibetan Plateau. *Journal of Climate*, *30*(15), 5699–5713.

Wu, J., & GAO, X.-J. (2013). A gridded daily observation dataset over China region and comparison with the other datasets. *Chinese Journal of Geophysics*, *56*(4), 1102–1111.

Xin, Y., Liu, J., Liu, X., Liu, G., Cheng, X., & Chen, Y. (2022). Reduction of uncertainties in surface heat flux over the Tibetan Plateau from ERA-Interim to ERA5. *International Journal of Climatology*, *42*(12), 6277–6292. https://doi.org/10.1002/joc.7589

Xu, X., Zhao, T., Lu, C., Guo, Y., Chen, B., Liu, R., et al. (2014). An important mechanism sustaining the atmospheric" water tower" over the Tibetan Plateau. *Atmospheric Chemistry and Physics*, *14*(20), 11287–11295.

Xu, X., Ma, Y., Sun, C., & Wei, F. (2019). Effect of energy and water circulation over Tibetan Plateau. *Bulletin of Chinese Academy of Sciences (Chinese Version)*, *34*(11), 1293–1305.

Yang, K., Tang, Q., & Lu, H. (2022). Precipitation recycling ratio and water vapor sources on the Tibetan Plateau. *Science China Earth Sciences*, *65*(3), 584–588. https://doi.org/10.1007/s11430-021-9871-5

Yao, T., Masson-Delmotte, V., Gao, J., Yu, W., Yang, X., Risi, C., et al. (2013). A review of climatic controls on 18O in precipitation over the Tibetan Plateau: Observations and simulations. *Reviews of Geophysics*, *51*(4), 525–548. https://doi.org/10.1002/rog.20023

Yao, T., Xue, Y., Chen, D., Chen, F., Thompson, L., Cui, P., et al. (2019). Recent Third Pole's Rapid Warming Accompanies Cryospheric Melt and Water Cycle Intensification and Interactions between Monsoon and Environment: Multidisciplinary Approach with Observations, Modeling, and Analysis. *Bulletin of the American Meteorological Society*, *100*(3), 423–444. https://doi.org/10.1175/BAMS-D-17-0057.1

Yao, T., Bolch, T., Chen, D., Gao, J., Immerzeel, W., Piao, S., et al. (2022). The imbalance of the Asian water tower. *Nature Reviews Earth & Environment*, 1–15. https://doi.org/10.1038/s43017-022-00299-4

Yasunari, T., & Miwa, T. (2006). Convective cloud systems over the Tibetan Plateau and their impact on meso-scale disturbances in the Meiyu/Baiu frontal zone: A case study in 1998. *Journal of the Meteorological Society of Japan*, *84*(4), 783–803. https://doi.org/10.2151/jmsj.84.783

Zhang, C. (2020a). Moisture source assessment and the varying characteristics for the Tibetan Plateau precipitation using TRMM. *Environmental Research Letters*, *15*(10), 104003. https://doi.org/10.1088/1748-9326/abac78

Zhang, C. (2020b). Moisture sources for precipitation in Southwest China in summer and the changes during the extreme droughts of 2006 and 2011. *Journal of Hydrology*, *591*, 125333. https://doi.org/10.1016/j.jhydrol.2020.125333

Zhang, C., Tang, Q., & Chen, D. (2017). Recent Changes in the Moisture Source of Precipitation over the Tibetan Plateau. *Journal of Climate*, *30*(5), 1807–1819. https://doi.org/10.1175/JCLI-D-15-0842.1

Zhang, C., Tang, Q., Chen, D., Ent, R. J. van der, Liu, X., Li, W., & Haile, G. G. (2019). Moisture Source Changes Contributed to Different Precipitation Changes over the Northern and Southern Tibetan Plateau. *Journal of Hydrometeorology*, *20*(2), 217–229. https://doi.org/10.1175/JHM-D-18-0094.1

Zhang, Y., Huang, W., & Zhong, D. (2019). Major Moisture Pathways and Their Importance to Rainy Season Precipitation over the Sanjiangyuan Region of the Tibetan Plateau. *Journal of Climate*, *32*(20), 6837–6857. https://doi.org/10.1175/JCLI-D-19-0196.1

Zhao, Y., & Zhou, T. (2021). Interannual Variability of Precipitation Recycle Ratio Over the Tibetan Plateau. *Journal of Geophysical Research: Atmospheres*, *126*(2), e2020JD033733. https://doi.org/10.1029/2020JD033733

Zhong, L., Ma, Y., Xue, Y., & Piao, S. (2019). Climate Change Trends and Impacts on Vegetation Greening Over the Tibetan Plateau. *Journal of Geophysical Research: Atmospheres*, *124*(14), 7540–7552. https://doi.org/10.1029/2019JD030481

Zhu, K., Xue, M., Zhou, B., Zhao, K., Sun, Z., Fu, P., et al. (2018). Evaluation of Real-Time Convection-Permitting Precipitation Forecasts in China During the 2013–2014 Summer Season. *Journal of Geophysical Research: Atmospheres*, *123*(2), 1037–1064. https://doi.org/10.1002/2017JD027445